Published in Polyhedron 27, issue 2, 623-632, 2008
which should be used for any reference to this work

Study of protonation and Zn(II), Cd(II), Cu(II) and Mn(II) complexation with a glutamic acid *N*-pyrimidine derivative: Crystal structure of a neutral Cd(II) complex of the bianionic ligand

P. Arranz-Mascarós [a], M.D. Gutiérrez-Valero [a], R. López-Garzón [a,*], M.D. López-León [a], M.L. Godino-Salido [a], A. Santiago-Medina [a], H. Stoeckli-Evans [b]

[a] *Department of Inorganic and Organic Chemistry, University of Jaén, 23071 Jaén, Spain*
[b] *Institute of Chemistry, University of Neuchâtel, CH-2007 Neuchâtel, Switzerland*

Abstract

The compound *N*-(4-amino-1-methyl-5-nitroso-6-oxo-1,6-dihydropyrimidin-2-yl)-(s)-glutamic acid (H_3L) was synthesised and structurally characterised by analytical methods and ^1H, ^{13}C and ^{15}N NMR spectroscopy. This compound (H_3L) shows the same topology as other model receptors previously used to develop chemical functionalization at the surface of an active carbon when they adsorb on it. Protonation of H_3L and its coordination ability towards Cd^{2+}, Zn^{2+}, Cu^{2+} and Mn^{2+} ions in water solution was also studied by potentiometric methods, UV–Vis and ^1H, ^{13}C NMR spectroscopies. The obtained results allow us to fit the operative conditions for the use of the activated carbon–H_3L adsorbent for the retaining of the above-mentioned metal ions in aqueous solutions. The molecular structure of $\{[Cd(HL)H_2O]\ \ 3H_2O\}_n$ was solved by single-crystal X-ray diffraction methods.

Keywords: Cadmium; Zinc; Manganese and copper complexes; Adsorption; Ligand design; Crystal structures

1. Introduction

Environmental contamination from a wide variety of sources has become an increasingly serious problem in recent years. Activated carbons have been extensively used for the purification or recovery of pollutant metals in waste waters [1–3]. In recent works [4,5], we have described a new method to add chemical functionality to the surface of an active carbon based on adsorbing the above-mentioned model compounds on it. That adsorption, which takes place when pyrimidine residues interact with carbon arene centres, favours adsorbed compounds acting as metal–ion receptors. This method provides specific chemical functionalization of the carbon surface provided by the substituent existing at the C2 position of the pyrimidine.

Previous results point out that in the case of analogous molecular compounds derived from single amino acids L-alanine, L-valine, L-methionine, L-serine and L-glycylglycine, the adsorption capacity of adsorbents AC-molecular receptors to different metal ions was improved in relation to AC. It was also proved that this fact is due to the metal-binding capacity of the carboxyl function existing at the C2 substituent [6].

The model compound *N*-2-(4-amino-1,6-dihydro-1-methyl-5-nitroso-6-oxo-pyrimidin,2-yl) L-glutamic acid, H_3L (Scheme 1), shows the metal binding bicarboxylate COO^-–CHR–CH_2–CH_2–COO^- at the C2 position of the pyrimidine moiety. Thus, it is expected that the metal binding ability of the amino acid residue would improve the

* Corresponding author. Tel.: +34 953212186; fax: +34 953211876.
E-mail address: rlopez@ujaen.es (R. López-Garzón).

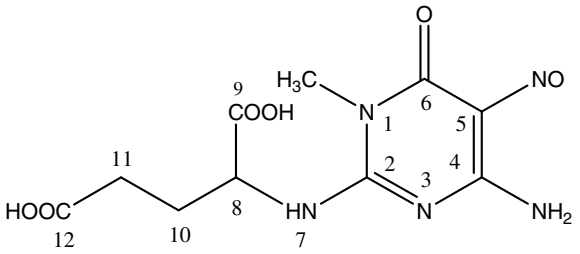

Scheme 1.

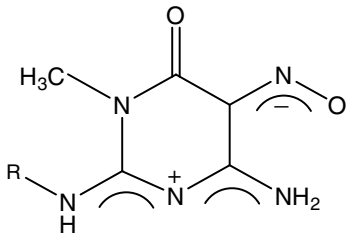

Scheme 2. Structure with charge delocalization

single monocarboxyl function existing at the single amino acid derivatives previously studied. In this work, we present the synthetic procedure for the H_3L compound and its structural characterization by thermal analysis, NMR and UV–Vis spectroscopy. The coordinating behaviour of H_3L to Zn(II), Cd(II), Cu(II) and Mn(II) metal ions has been recognized by studying the reactivity of the different H_3L/metal systems. The aim of this recognition was establishing the experimental conditions at which the bi-carboxyl function of the adsorbed ligand on an activated carbon is operative to metal ions, and also providing the thermodynamic properties of such a function for the above-mentioned metal ions. Reactivity studies were carried out using potentiometric, ^{13}C NMR and UV–Vis methods. The structure of the $\{[Cd(HL)H_2O]\cdot 3H_2O\}_n$ complex, which was solved by X-ray single crystal methods [7], is also reported.

2. Results and discussion

2.1. Synthesis and characterization of the molecular receptor

H_3L was prepared by a synthetic procedure [8] consisting of condensation of L-glutamic acid and 4-amino-1,6-dihydro-1-methyl-5-nitroso-6-oxo-pyrimidine [8,9]; this reaction takes place by the nucleophilic attack of the α-NH_2 amino group of L-glutamic acid on the C2 atom of the pyrimidine [8,9]. The structure of H_3L was determined by ^1H–^1H, ^1H–^{13}C and ^1H–^{15}N bi-dimensional spectra (see Section 4). Assignments are in accordance with the structural data of the H_3L unit, which were obtained by single X-ray diffraction methods [8].

The pyrimidine moiety shows alike structural and electronic features to a series of analogous compounds obtained by condensation of the above-mentioned pyrimidine derivatives with a series of single amino acids [10]. These data show extensive π-electron delocalization at the cyclic moiety which also involves the C2NH_2, C6O, C5NO and C4NH_2 exocyclic substituents. The somewhat long bond length values in the NH–C2–N3–C4–NH_2 fragment and the short bond distances in the C5NO grouping point out the location of a positive charge at the former fragment, and a negative charge at the latter; for example, the bipolar character of the aromatic moiety. These features have already been observed in the case of analogous amino acid derivatives [10] (Scheme 2).

2.2. Ligand protonation

The Brönsted acid–base behaviour of H_3L in aqueous solution was studied as a previous step on the study of the reactivity of the H_3L/metal ion systems in aqueous solutions. The protonation pattern of the ligand was also determined by following the dependence of the ^{13}C NMR signals of a H_3L solution on pH.

The protonation equilibrium of the ligand in solution (0.1 mol dm^{-3}KCl, 25 °C) within a 2.5–10.5 pH range was determined by a potentiometric method (see Section 4) and results are reported in Table 1.

Distribution plots of the protonated species of the ligand were obtained from the data of Table 1 and are shown in Fig. 1. The tri-anion L^{3-}, which exists at high pH values, binds four protons in the pH range investigated (2.0–10.5).

Table 1
Protonation constants ($\log K$) of the ligand H_3L (0.1 mol dm^{-3} KCl, 298.1 K)

Reaction	$\log K$[a]
	H_3L
$L^{3-} + H^+ = [HL]^{2-}$	12.11 (2)
$[HL]^{2-} + H^+ = [H_2L]^-$	4.43 (3)
$[H_2L]^- + H^+ = [H_3L]$	3.00 (1)
$[H_3L] + H^+ = [H_4L]^+$	1.90 (2)

[a] Values in parentheses are standard deviations in the last significant number.

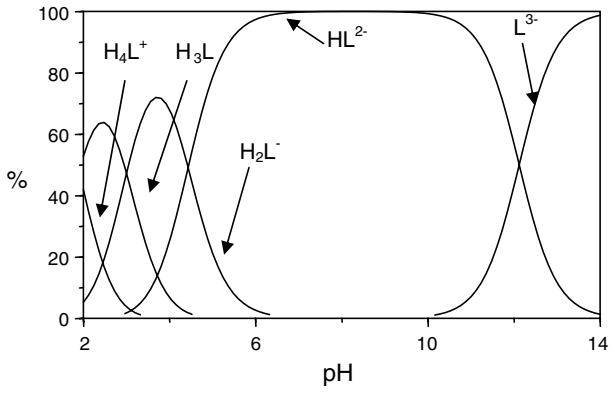

Fig. 1. Distribution species diagram as a function of pH for the ligand H_3L (10^{-3} mol dm^{-3}) in aqueous solution (0.1 mol dm^{-3} KCl) at 298.1 K.

The $\log K_{HL}$ value corresponding to the protonation of the tri-anion, $L^{3-} + H^+ = HL^{2-}$ (12.12), indicates that the corresponding binding site is strongly basic. The two protonation processes corresponding to the neutralization of the resulting bi-anion markedly overlap (see Fig. 1), and their matching constants are found within the expected range for the protonation of the two carboxylate residues existing at the *F* function of the ligand [11] ($\log K_{H_2L} = 4.43$, $\log K_{H_3L} = 3.00$). Bearing in mind the presence of a long spacer between terminal carboxylate groups, their basicities should be analogous; therefore the differences between both $\log K$ values can be attributed to statistical effects [12]. Finally, a protonation step corresponding to the $H_3L + H^+ = H_4L^+$ equilibrium (with $\log K_{H4L} = 1.9$) points out the very weak basic character of the corresponding proton binding site.

The addition of two protons to the HL^{2-} species, which takes place under the pH range 3–7 (see Fig. 1), does not produce any change in the UV–Vis spectrum of the ligand. On the other hand, as shown in Fig. 2, an increasing shielding of the ^{13}C NMR signal corresponding to the CH_2 groups at positions 8, 10 and 11 and of the two C atoms of the carboxyl groups (C(9) and C(12)) is observed in the above pH range as the pH decreases, indicating the protonation of the two COO^- anions.

The onset of H_3L protonation, which takes place at pH 3.5 (Fig. 1), is accompanied by changes in the UV and visible spectra of the compound (Fig. 3). Among these changes, the vanishing of a band at 524 nm stands out, which is assigned to a forbidden $n_N \rightarrow \pi^*$ transition of the C5NO chromophore (see Fig. 3), indicating that the protonation site is the nitrogen atom of the above mentioned group [13,14].

Deprotonation of HL^{2-}, which onsets at pH ca. 10.32, is accompanied by UV and visible spectral changes (see Figs. 1 and 3). Moreover this process is accompanied by significant shifts of the C(2) signal in the ^{13}C NMR spectra of H_3L, suggesting that the group involved in this protonation

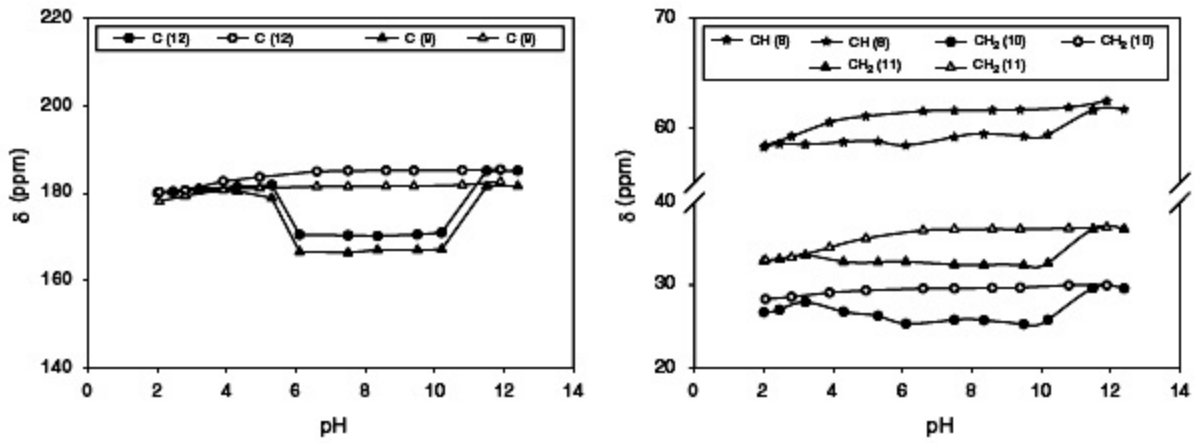

Fig. 2. ^{13}C NMR chemical shifts of C(8), C(10), C(11) and C(12) carbon atoms vs. pH of an H_3L D_2O solution (white points) and an H_3L/Cd^{2+} (1/1 molar ratio) D_2O solution (black points).

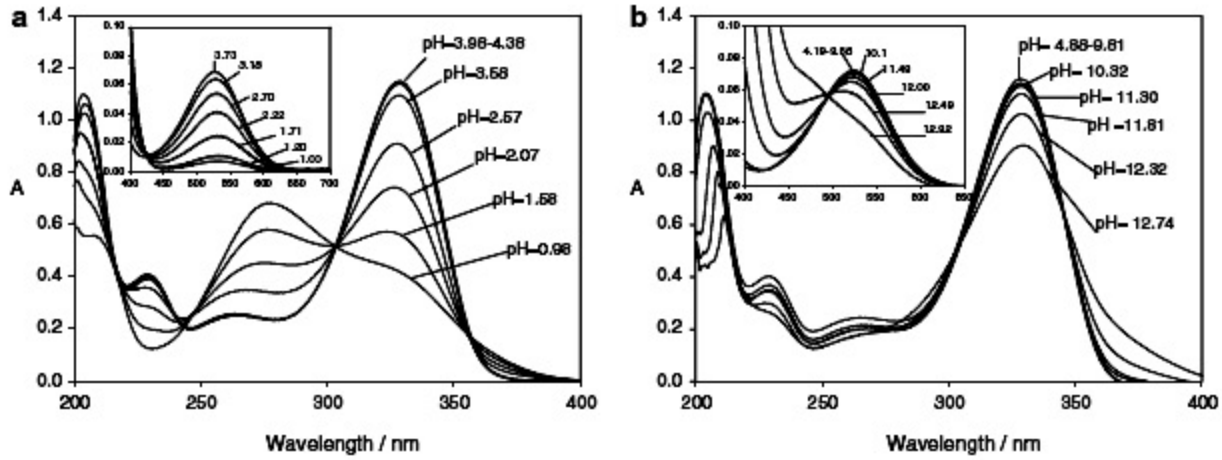

Fig. 3. pH-Dependence of the absorption spectra of H_3L in the UV ($[H_3L] = 5 \times 10^{-5}$ mol dm^{-3}, 0.1 mol dm^{-3} KCl), and visible ($[H_3L] = 10^{-3}$ mol dm^{-3}, 0.1 mol dm^{-3} KCl) regions, (a) in acidic media and (b) in basic media.

step is C2HN, which is conjugated with the pyrimidine moiety.

2.3. Complex formation in aqueous solution

As it has been previously said [4–6], the main adsorption mechanism of ligands analogous to H_3L and also of the H_3L ligand [15] on the activated carbon involves a plane-to-plane interaction between the pyrimidine moiety of the former and the arene centres of the graphite planes of the AC. This kind of interaction blocks the basic functions of the pyrimidine moiety, limiting the reactivity of the ligand (AC–H_3L) anchored with metal–ions to that of the amino acid residue of H_3L. Therefore, the main objectives of the studies of ligand–metal ion complex formation in solution are to obtain the data necessary to fit pH conditions at which the bi-carboxyl function of the anchored H_3L are operative for metal–ion binding, and also determine its coordinating ability to these ions, (i.e., to characterize its coordination patterns and stabilities) which would state the metal adsorption capacities of the AC–H_3L adsorbent.

The complex formation equilibria and the corresponding constants in aqueous solutions for the studied H_3L/metal ion systems were obtained from the potentiometric-titration data of the corresponding ligand/metal ion mixtures ([H_3L]/[metal ion] = 1/1), which were processed with the HYPERQUAD software [16]. The best fit of the experimental data for each of the studied systems corresponds to those summarized in Table 2. The corresponding species distribution plots appear in Fig. 4.

Data displayed in Table 2 and Fig. 4 highlight that the highest reactivities and the most stable complexes are displayed in ligand/Cu^{2+} and ligand/Cd^{2+} systems, whereas the lowest are shown in the ligand/Mn^{2+} system.

In all the studied systems, mononuclear complexes showing 1/1 ligand/metal–ion stoichiometries are formed, even though the ligand can be found in the following forms: neutral (H_3L), monoanionic (H_2L^-), bianionic (HL^{2-}) and trianionic (L^{3-}). Additionally, a mononuclear complex with a 2/1 ligand to metal–ion stoichiometry is formed in the case of the ligand/Cd^{2+} system. Moreover, binuclear complexes (e.g., with 1/2 ligand/metal–ion stoichiometries) which contain the ligand partially deprotonated, as the bi and/or

Table 2
Equilibrium constants (0.1 mol dm^{-3} KCl, 298.1 K) for Cu(II), Zn(II), Cd(II) and Mn(II) complexes with H_3L in aqueous solution

Reaction	log K			
	Cu(II)	Zn(II)	Cd(II)	Mn(II)
$M^{2+} + L^{3-} \rightleftarrows [M(L)]^-$	10.71			
$M^{2+} + HL^{2-} \rightleftarrows [M(HL)]$	4.18	2.41	3.95	
$M^{2+} + H_2L^- \rightleftarrows [M(H_2L)]^+$	3.98	2.70		2.31
$M^{2+} + H_3L \rightleftarrows [M(H_3L)]^{2+}$	3.75		3.76	
$2M^{2+} + H_2L^- \rightleftarrows [M_2(H_2L)]^{3+}$			7.88	
$2M^{2+} + HL^{2-} \rightleftarrows [M_2(HL)]^{2+}$	6.68	5.82	7.26	5.92
$M^{2+} + HL^{2-} + L^{3-} \rightleftarrows [M(HL)L]^{-3}$			10.15	
$M^{2+} + L^{3-} + OH^- \rightleftarrows [M(L)(OH)]^{2-}$	16.49			
$M^{2+} + 2OH^- \rightleftarrows M(OH)_2$		−14.03	−16.61	−17.95

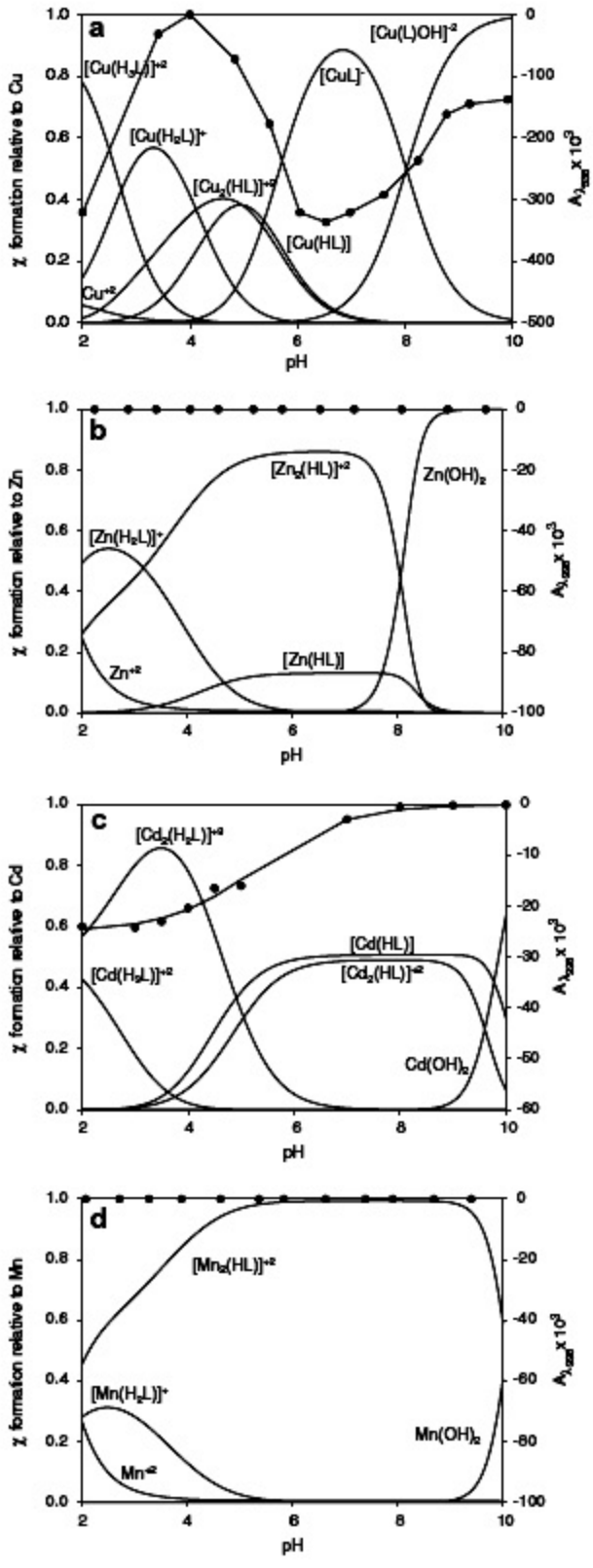

Fig. 4. Distribution species diagrams and absorbance differences at λ = 338 nm (black points, see text) with pH function systems for: (a) H_3L/Cu(II), (b) H_3L/Zn(II), (c) H_3L/Cd(II) and (d) H_3L/Mn(II) (1:1 molar ratio, 0.1 mol dm^{-3} KCl and 298.1 K).

mono-anion, are also detected. Table 2 shows that the highest reactivity corresponds to the Cu^{2+}/ligand system, whereas a poor speciation is found in the Mn^{2+}/ligand system.

Mononuclear complexes containing the fully protonated ligand H_3L are detected in the cases of Cu^{2+} and Cd^{2+} ions. As is expected, it can be seen in Fig. 4 that these complexes are the main species existing in the pH range under 4. Bearing in mind the poor nature of coordination of carboxyl groups and the N3 atom of the pyrimidine to metal–ions [5,13,14,17,18], single positions of the H_3L ligand available for binding to metal ions are the C5NO and C6O groups of the aromatic residue. Thus, it is expected that in complexes of the $[M(H_3L)]^{2+}$ type detected ($M^{2+} = Cu^{2+}$ and Cd^{2+}), H_3L behaves as a chelating bidentate ligand, using the N atom of C5NO and the O atom of C6O as binding positions to the mentioned metal ions. Otherwise, this behaviour is consistent with analogous pyrimidine derivatives, having the substituents –NO and =O at the C5 and C6 positions, respectively. In fact, the stability constants of $[CuH_3L]^{2+}$ and $[CdH_3L]^{2+}$ ($\log K = 3.75$ and 3.76 respectively, see Table 2) are in a similar range to those found for Cu^{2+} and Cd^{2+} complexes, with analogous C5-nitroso C6-oxo derivatives [18].

Deprotonation of H_3L species in the H_3L/metal ion system takes place at slightly lower pH values than in a water solution of the ligand. This fact produces the formation of binuclear $[M_2H_2L]^{3+}$ and/or mononuclear $[MH_2L]^{+}$ species. The former is only detected in the case of the H_3L/Cd^{2+} system (see Fig. 4). In the remaining three systems, these binuclear species are not detected, but mononuclear complexes $[MH_2L]^{+}$ are formed. Log K_{MH2L} values for the association of Cu^{2+}, Zn^{2+}, Cd^{2+} and Mn^{2+} to the carboxylate group in these complexes are similar to those described in the literature for single carboxylate ligands [5,13,14,17–21]. The onset of the deprotonation of the remaining carboxyl functions of H_2L^{-} occurs at higher pH values than the domain of H_2L^{-} complex species, giving rise to mono- and binuclear [MHL] and $[M_2HL]^{2+}$ complexes, respectively. The former is detected in all systems, excluding the Mn^{2+}/ligand system, whereas the second is detected in all systems. The formation of $[M_2HL]^{2+}$ metal complexes suggests that the anchorage of the H_3L ligand on an activated carbon surface would improve the metal–ion capture capacity showed by similar ligands having a C2-substituent with a mono-carboxyl function [6]. In fact, previous results, obtained in the study of the Cu^{2+} adsorption by an H_3L–AC adsorbent, strengthen this hypothesis [15].

It is noteworthy that the calculated $\log K_{MHL}$ values for a given metal ion are very alike to those corresponding to $[MH_2L]^{+}$ complexes (see Table 2), which demonstrate that the coordination of HL^{2-} to the metal–ions in the detected MHL complexes only takes place through one of the two carboxylate groups, whereas the second probably remains uncoordinated. This fact can be due to the low stability of the seven-membered chelate ring, which would result from a cooperative binding of the two carboxylate functions to the same metal ion. However, more stable $[M_2HL]^{2+}$ complexes containing two metal ions coordinated to each of the two carboxylate groups are formed.

Species distribution plots of the Cu^{2+}/ligand system (Fig. 4a) show the formation of CuL^{-} and $CuLOH^{2-}$ metal complexes in the upper pH range, which holds the fully deprotonated L^{3-} anion as a ligand. It is also noteworthy in this system that the onset of the formation of the CuL^{-} species takes place at pH ca. 4, which is a lot lower than that determined for the deprotonation of HL^{2-} in water, which is ca. 10 (Fig. 1). This fact is due to the electron-withdrawing character of Cu^{2+} which induces early deprotonation of the HL^{-} species. The high Log K_{CuL} and $\log K_{CuLOH}$ values probably point out the role of the $C2_{py}N^{-}$ group as a binding site to the metal ion, together with one of the carboxylate groups.

To get further insight into the coordinating behaviour of H_3L, we carried out a spectrophotometric titration in the visible range of an aqueous 1/1 ligand/Cu^{2+} mixture. Fig. 5 shows the spectra obtained at given pH values by

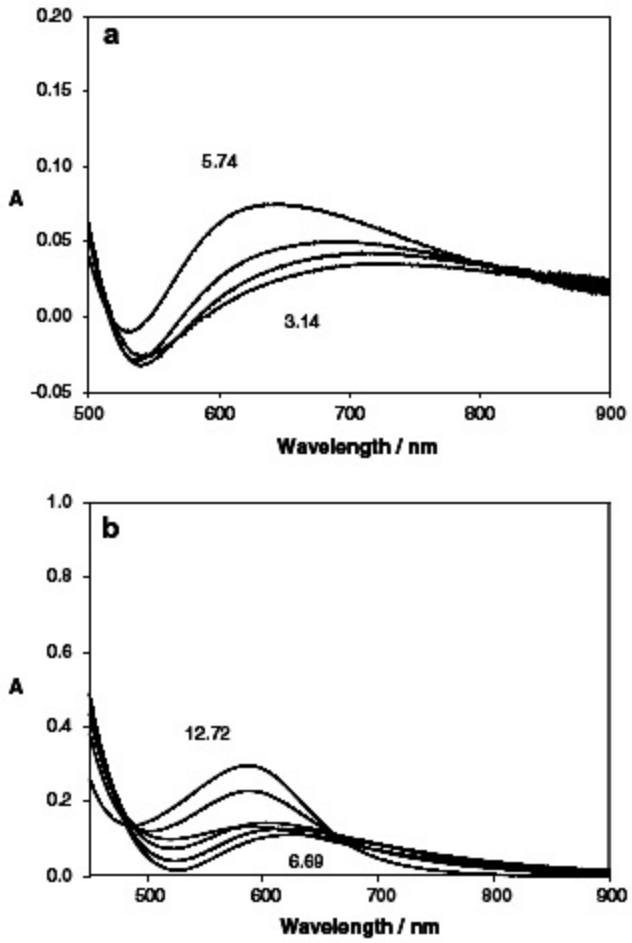

Fig. 5. Spectral curves of the ligand/Cu system in the visible range vs. pH ($[H_3L] = 10^{-3}$ mol dm^{-3}, 0.1 mol dm^{-3} KCl): (a) acidic medium from pH 3.14 to 5.74 (top), (b) basic medium from pH 6.69 to 12.72 (top).

subtracting those of H_3L from the corresponding 1/1 ligand/Cu^{2+} mixtures in aqueous solution.

In the lowest pH range, in which the main complex species existing in solution is $[CuH_3L]^{2+}$, the observed negative absorbance-values at the characteristic wavelength of the forbidden $n_N \rightarrow \pi^*$ transition of the C5NO chromophore ($\lambda_{max} = 524$ nm, see above) point out the blocking of the *n* electron pair of the N atom of such a group. This fact indicates that, in the $[CuH_3L]^{2+}$ complex, the Cu^{2+} ion is coordinated to the nitroso group of the pyrimidine. Moreover, a wide weak band with a λ_{max} value of ca. 700 nm indicates a weak ligand field in this complex.

As the pH increases within the 3–5 range, the concentration of the $[CuH_3L]^{2+}$ complex diminishes until it vanishes at the last pH value, and the $[CuH_2L]^{+}$, $[Cu_2HL]^{2+}$ and CuHL COO^--coordinated complexes increase, becoming the main ones, as Fig. 4 illustrates. The disappearance of the $[CuH_3L]^{2+}$ complex, in which the Cu^{2+} ion is coordinated through the C5NO group, explains the vanishing of the absorbance minimum at 524 nm in the mentioned 3–5 pH range in the spectra of Fig. 5, while the formation of more stable COO^--coordinated complexes explains the shifting of λ_{max} due to the d → d transition to values lower than the above mentioned 700 nm. It can also be seen in Fig. 5 that this shifting continues steadily as pH increases within the 6–12 pH range, reflecting the formation of more stable complexes: $[CuL]^-$ (the only species existing at a pH value of ca. 6.7) and $[CuLOH]^{2-}$, which is the unique complex existing at pH values up to 10.

To get further information on the coordination models of the ligand to the metal ions a series of NMR experiments with various ligand/metal ions mixtures have been performed. As was said above, the metal ions coordination to the N atom of the C5NO group can be enhanced by the disappearance of a characteristic absorption band of this group in the visible range. This weak band, which appears at 525 nm in the H_3L spectrum, is due to a n → π transition of the σ non-bonding pair of the mentioned N atom [18].

Fig. 6 shows the vanishing of the mentioned 525 nm band with the addition of growing amounts of Cu^{2+} to an H_3L aqueous solution at a constant pH 2.0. This fact proves that the N atom of the C5–NO group act as a binding site in the mononuclear CuH_3L complex formed at this pH value (see Fig. 4a). Due to conjugation of the C5-nitroso group with the pyrimidine moiety, metal coordination to the C5NO group induces electronic changes in the conjugated moiety of the H_3L molecule. These changes explain also the variations observed in the strong intensity bands (which are due to allowed $\pi \rightarrow \pi^*$ transitions) of the UV spectrum of an H_3L water solution (see Fig. 6) under the addition of increasing amounts of Cu^{2+} at a constant pH 2. Thus, it would be expected that the binding of some of the conjugated basic atoms of H_3L to metal ions in the complexes formed in water solution (i.e. in the cases of $[Cu H_3L]^{2+}$, $[Cd H_3L]^{2+}$ and $[CuL]^-$) would be accompanied by clear changes in the UV spectrum. On the contrary the metal ion complexes of H_2L^- and HL^{2-} in which carboxylate anions act as binding sites would not induce such changes in the UV spectrum of the ligand.

Thus, the differences between the UV spectra of a ligand/Cu^{2+} mixture with a 1:1 molar ratio and the ligand alone ($[ligand] = 5 \times 10^{-5}$ mol dm^{-3}) in water solution were obtained at several pH values in the 2.5–10 pH range. The maximum differences in absorbance values are found at a λ value of ca. 338 nm. Insignificant differences in the whole UV range were found in a narrow pH window centred at pH 4. This observation is consistent with the hypothesis established through the potentiometric data, that in the main complex species existing at these pH values ($[CuH_2L]^+$, $[Cu_2HL]^{2+}$ and [CuHL], (see Fig. 4a)) the coordination of the ligands would take place through the carboxylate groups. On the contrary, as the pH values decrease in the 4.0–2.5 pH range, increasing negative differences in the absorbance values at 338 nm are observed in the difference spectra. The last observation is consistent with the fact that the amount of $[CuH_3L]$ (the species in which the H_3L ligand is NO-coordinated) increases with decreasing pH values in that pH range. In the same way the trends of differences in the absorbance values observed in the 4 to 10 pH range, are also consistent with the forma-

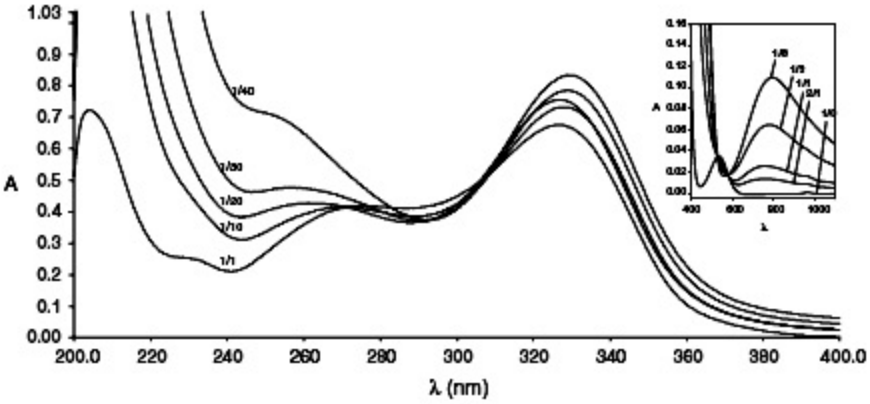

Fig. 6. [Cu] Variations of the visible and UV spectra of an H_3L/Cu^{2+} mixture with variable H_3L:Cu^{2+} molar ratio values at constant pH 2.

tion of $[CuL]^-$ and $[CuLOH]^{2-}$ complexes, which contain the L^{3-} ligand, coordinated through the conjugated N^- atom of the deprotonated amine group attached to $C(2)_{pyr}$.

In the case of the ligand/Cd^{2+} system, the difference spectra shows a negative band at ca. 338 nm in the 2.5–6.0 pH range whereas zero absorbance is obtained in the whole UV region in the 6–10 pH range (see Fig. 6c). The shape of the plot of the absorbance difference values versus pH at the above wavelength is consistent with the potentiometric hypothesis. Thus, the appearance of a band at 338 nm in the UV difference spectra in the low pH range indicates that in the main existing species $[Cd_2(H_2L)]^{3+}$ and $[Cd(H_3L)]^{2+}$the ligand interacts with the metal ion through the N atom of the C(5)NO group. On the contrary, zero absorbance values in the pH range corresponding to values higher than 4 indicate that in [Cd(HL)] and $[Cd(H_2L)]^+$ complexes the ligand is not coordinated to Cd^{2+} through any of the conjugated basic atoms. Fig. 2 shows the plots of the chemical shift values of the carbon signals of the three methylene and the carboxyl groups of the amino acid moiety versus the pH values. These were obtained by the NMR titration of an H_3L/Cd^{2+} mixture as described in the experimental section. Fig. 2 shows that the onset of the formation of [Cd(HL)] and $[Cd(H_2L)]^+$ complexes taking place at a pH value of ca. 3 (see Fig. 4c) is accompanied by the shielding of the methylene carbon atoms and also the carboxyl ones. This indicates the existence of a carboxylate–Cd^{2+} interaction in the above complexes. The observed shielding, which is clearly stronger for the carboxylate groups than for methylene, can be explained by the stronger ionic character of the carboxylate–Cd^{2+} interaction than the carboxylate–proton one.

Very different behaviour is observed in the cases of the H_3L/Zn^{2+} and H_3L/Mn^{2+} systems in aqueous solutions. The difference spectra of both systems, in the 200–400 nm UV region were obtained in the 2.3–10.5 pH range and in the 2.7–10.1 pH range, respectively. The negligible differences in absorbance observed in all of the wavelength range in the two systems prove that complexes having the ligand coordinated through the basic conjugated atoms are not formed in any of the two systems. This proves that complexes detected in the potentiometric studies of these two systems, contains the ligands coordinated through the carboxylate groups (see above).

2.4. Conclusions

The results obtained from the above reactivity studies have provided the needed information (see above) to further interpret the adsorption properties to metal ions of the anchored ligand at the graphitic surface of activated carbon [15]. The whole reactivity data point out that H_3L behaves as a bi-functional ligand. In the low pH range, the only operative function is the C6O–C5NO grouping. This supports the formation of the five-member chelate complexes detected in this pH range with all the studied metal ions, excluding the Mn^{2+} and Zn^{2+} ions. In the last cases, the potentiometric and UV spectroscopic data ruled out the formation of a complex of this type. Nevertheless, the crystal structure of a Mn^{2+} complex with a pyrimidine analogue of H_3L with the methionine residue at the C2 cyclic atom [13], shows a supramolecular assembly in which COO^- coordinated Mn^{2+} ions of each unit interacts with the oxygen atom of the C5NO group of the pyrimidine moiety. All the previous data points out the possibility of the formation of a Mn^{2+} complex in the low pH range (also in the H_3L/Mn^{2+} system), in which the metal ion would be weakly coordinated to the pyrimidine moiety in a similar way. If so, the lack of protic properties of the oxygen atom of the NO group, would be the reason why this complex was not detected with the potentiometric method used in this work.

The deprotonation of the carboxyl functions of the substituent at $C2_{py}$ of the pyrimidine taking place in the intermediate pH range involves the availability of the carboxylate groups as operative basic functions for the binding to metal–ions. This leads to the formation of mono- and binuclear metal complexes within this pH range, in which one or two of the COO^- functions are coordinated to one or two metal ions respectively. Nevertheless, within this pH range, also binuclear complexes of H_2L^- ligand, containing one of the metal ions coordinated to the pyrimidine moiety and the second to a COO^- function, are also formed in the case of the Cd^{2+}/ligand system. Finally, in the highest pH range of all studied systems, the ligand uses one of the two carboxylate groups as a coordinating basic site, although cooperative coordination of both of them to the same metal–ion does not occur. In the case of the Cu^{2+} ion, the ligand also uses the $C2_{py}$-N^- group as a binding site, together with a COO^- group forming chelate complexes. It is noteworthy that the $N3_{py}$ position displays no affinity to any of the studied metal–ions. This fact, which is consistent with previous observations done with other analogous pyrimidine derivatives [5,19], agrees with the typical low electron density existing at the $–NH–(C2–N3–C4)_{py}–NH_2$ moiety [8,10].

In the species distribution diagrams of all the studied systems, it is seen that the deprotonation pH of the most acidic carboxyl groups (those of formation of $[M_2H_2L]^{3+}$ and/or $[M_2HL]^{2+}$ species) takes place at pH values meaningfully lower than those corresponding to the free ligand (see Fig. 1). These results bring up to date the pH values at which the H_3L ligand anchored on the graphite moiety of an AC (the H_3L–AC adsorbent) would be operative for the adsorption of metal ions in aqueous solution, although the expected optimum values would be those corresponding to the maximum of the plots for the metal-complexes with the fully deprotonated carboxyl functions, $[M_2HL]^{2+}$ and [MHL].

3. Crystal structure of $\{[Cd(HL)H_2O] \cdot 3H_2O\}_n$

The crystal structure of the complex $\{[Cd(HL)H_2O] \cdot 3H_2O\}_n$ was solved by single X-ray diffraction methods. A view of the asymmetric unit and the crystal packing is

depicted in Fig. 7, and selected bond and angles are listed in Table 3.

The compound consists of 2D molecules containing equivalent hepta-coordinated Cd^{2+} centres, each of which is coordinated to one water molecule, to two carboxylate groups of two individual HL^{2-} molecules (acting as bidentate chelating ligands with the two oxygen atoms in binding position), and to a third HL^{2-} molecule (also acting as a chelating ligand), using the N atom of the C5NO group and the O atom of the C6O of the pyrimidine moiety as binding sites. Thus, as shown in Fig. 7, HL^{2-} anions act as bridging ligands to three different Cd^{2+} ions using the pyrimidine moiety and the two carboxylate groups as binding moieties, as it has been previously said. The resulting structure around the Cd^{2+} ions can be described as a strongly distorted bipyramid. The distances of the metal ion to the five atoms (the O1, N4, O6, O5 and O3 atoms) in the equatorial plane are similar, and Cd–O3 bonds are widely deviated from the plane. On the other hand, the distances of atoms placed at the apical positions (O4 and O1W), which are also be very alike, are however shorter than the equatorial distances.

The 2D molecules are extended parallel to the *c* axis and are stacked parallel to one another along the *a* axis. Non-coordinated water molecules are placed in the inter-planar space, contributing to the stabilization of the 3D framework through their involvement in hydrogen bonding between neighbour molecular planes.

Concerning the organic ligand, it is noteworthy that the N3 cyclic atom of the pyrimidine does not act as donor atom, as observed in several structures of metal complexes of analogous ligands [14,18,22–25]. This fact is in agreement with the dipolar character of the pyrimidine moiety of the H_3L ligand [8].

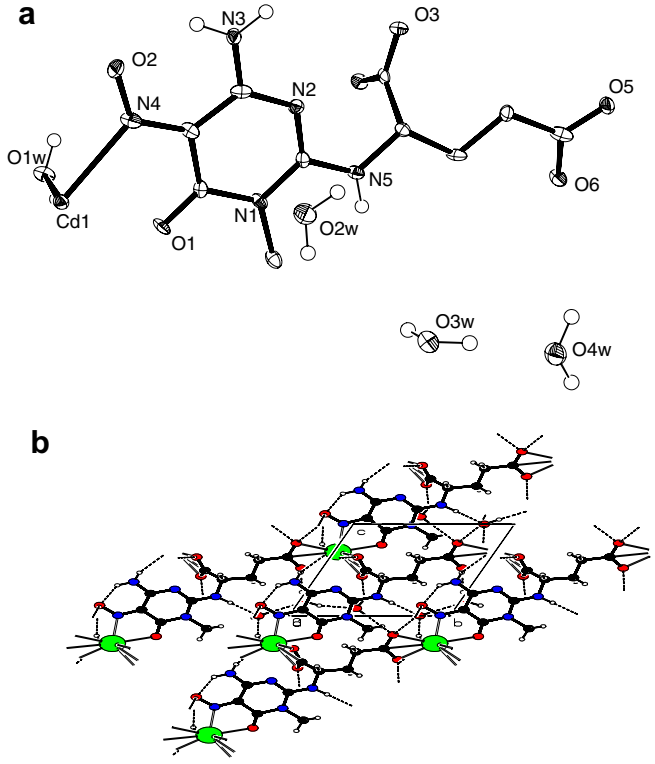

Fig. 7. (a) Drawing of the asymmetric unit, and (b) packing with the view of along arranged planes for $\{[Cd(HL)H_2O]\cdot 3H_2O\}_n$.

Table 3
Selected bond lengths (Å) and bond angles (°) for $\{[Cd(HL)H_2O]\cdot 3H_2O\}_n$

Bond lengths		Bond angles	
{[Cd(HL)H₂O]·3H₂O}ₙ			
O(1)–C(1)	1.218(5)	O(1W)–Cd(1)–O(4)	160.97(7)
O(2)–N(4)	1.277(4)	O(1W)–Cd(1)–O(5)	86.36(9)
N(1)–C(4)	1.371(4)	O(4)–Cd(1)–O(5)	97.02(9)
N(1)–C(1)	1.384(4)	O(1W)–Cd(1)–N(4)	91.85(9)
N(1)–C(5)	1.461(4)	O(4)–Cd(1)–N(4)	99.47(7)
N(2)–C(4)	1.310(5)	O(5)–Cd(1)–N(4)	132.26(7)
N(2)–C(3)	1.333(7)	O(1W)–Cd(1)–O(1)	86.02(11)
N(3)–C(3)	1.328(4)	O(4)–Cd(1)–O(1)	83.94(11)
N(4)–C(2)	1.327(4)	O(5)–Cd(1)–O(1)	157.94(10)
N(5)–C(4)	1.322(5)	N(4)–Cd(1)–O(1)	68.69(11)
N(5)–C(6)	1.465(4)	O(1W)–Cd(1)–O(3)	106.69(9)
C(1)–C(2)	1.462(5)	O(4)–Cd(1)–O(3)	55.42(8)
C(2)–C(3)	1.433(6)	O(5)–Cd(1)–O(3)	83.85(9)
		N(4)–Cd(1)–O(3)	141.07(9)
Cd(1)–O(1W)	2.297(2)	O(1)–Cd(1)–O(3)	78.58(10)
Cd(1)–O(4)	2.299(2)	O(1W)–Cd(1)–O(6)	102.33(9)
Cd(1)–O(5)	2.345(3)	O(4)–Cd(1)–O(6)	94.75(9)
Cd(1)–N(4)	2.383(3)		
Cd(1)–O(1)	2.416(4)		
Cd(1)–O(3)	2.438(2)		
Cd(1)–O(6)	2.456(2)		
Cd(1)–C(7)	2.696(3)		
Cd(1)–C(10)	2.746(5)		

4. Experimental

4.1. Reagents

The anhydrous ligand, H_3L ($C_{10}H_{13}N_5O_6$), was obtained by a synthetic method previously reported [8]. Nanopure water was used as the solvent for potentiometric and spectrophotometric measurements. Standardised KOH, HCl, $ZnCl_2$, $CuCl_2$ and $MnCl_2$ aqueous solutions (Merck) were also used. All the potentiometric measurements were carried out in 0.1 mol dm^{-3} KCl as the background electrolyte.

4.2. Synthesis of $\{[Cd(HL)H_2O]\cdot 3H_2O\}_n$

$CdCl_2\cdot 2\cdot 1/2\cdot H_2O$ (114.17 mg, 0.5 mmol) was added to a solution of H_3L (149.5 mg, 0.5 mmol). This solution was left to evaporate over a few days in air until orange crystals suitable for X-ray analysis were formed. *Anal.* Calc. for $C_{10}H_{13}CdN_5O_7$ 3(H_2O): C, 24.94; H, 3.97; N, 14.54. Found: C, 25.20; H, 3.99; N, 14.97%.

4.3. X-ray structure analyses

Details for data collection and structure refinement are summarized in Table 4.

Table 4
Crystal data and structure refinement for $\{[Cd(HL)H_2O]\cdot 3H_2O\}_n$

Empirical formula	$C_{10}H_{13}N_5O_{10}Cd$
Formula weight	481.70
T (K)	293(2)
Wavelength (Å)	0.71073
Space group	$P\bar{1}$
a (Å)	6.4653(12)
b (Å)	8.2956(15)
c (Å)	8.7113(15)
α (°)	65.794(19)
β (°)	73.47(2)
γ (°)	82.88(2)
V (Å^3)	408.51(13)
Z	1
D_{calc} (g cm^{-3})	1.958
μ (cm^{-1})	0.71073
Total reflections	3179
R^a	0.0288
Rw^b	0.0203

[a] $R = \sum(|F_o| - |F_c|)\sum|F_o|$.
[b] $Rw = [|\sum w(|F_o| - |F_c|)^2|\sum w|F_o|^2|]^{1/2}$.

4.4. X-ray structure of $\{[Cd(HL)H_2O]\cdot 3H_2O\}_n$

Suitable crystals of $\{[Cd(HL)H_2O]\cdot 3H_2O\}_n$ were obtained as orange block-like crystals by slow evaporation of an aqueous solution. The intensity data were collected at 153 K on a Stoe Image Plate Diffraction System [26] using Mo Kα graphite monochromated radiation. Image plate distance 70 mm, ϕ oscillation scans 0–200°, step $\Delta\phi = 2.0°$, 2θ range 3.27–52.1°, d_{min}–d_{max} = 12.45–0.81 Å. The structure was solved by direct methods using the program SHELXS-97 [7]. The refinement and all further calculations were carried out using SHELXL-97 [7]. The NH and NH_2 H atoms were located from difference Fourier maps and refined isotropically. The water molecule H atoms could be located from difference Fourier maps but in the final cycles of refinement they were constrained to be 0.86 Å and their U_{iso} thermal parameters = $1.5U_{eq}$(O atom). The remainder of the H atoms were included in calculated positions and treated as riding atoms using SHELXL default parameters; CH_3 = 0.98 Å, CH_2 = 0.99 Å, CH = 1.00 Å and $U_{iso} = 1.5(CH_3)$ or $1.2U_{eq}$(parent C atom). The non-H atoms were refined anisotropically, using weighted full-matrix least-squares on F^2.

An empirical absorption correction was applied using the DELrefABS subroutine in PLATON [27]; transmission factors T_{min}/T_{max} = 0.426/0.808.

The molecular structure and crystallographic numbering scheme are illustrated in the PLATON [27] drawing (see Fig. 6).

4.5. Potentiometric measurements

All potentiometric measurements ($pH = -\log[H^+]$) were carried out in degassed 0.1 mol dm^{-3} KCl solutions at 298.1 ± 0.1 K, with a 713 Methrom pH-mV meter, equipped with a combined glass electrode and connected to a Methron 765 Dosimat autoburette (1 ± 0.001 mL). The experimental procedure used was the same as that described elsewhere [28]. Typically, (1–1.5) × 10^{-3} mol dm^{-3} ligand concentration and 1:1 ligand/metal molar ratios were employed in the potentiometric measurements. At least four titration experiments (150 data points each) were carried out in the pH range between 2.5 and 10.5. The HYPERQUAD software [16], was used to calculate the equilibrium constants from the emf data.

4.6. Spectrophotometric measurements

Adsorption spectra were recorded on a Perkin–Elmer Lambda-19 spectrophotometer. H_3L spectra were obtained from 5×10^{-5} mol dm^{-3} aqueous solutions in the UV range and from 10^{-3} mol dm^{-3} aqueous solutions in the visible range (μ = 0.1 mol dm^{-3} KCl).

UV difference spectra were obtained using metal ion/H_3L mixtures with 1:1 molar ratios in aqueous solutions ($[H_3L] = 5 \times 10^{-5}$ mol dm^{-3}; μ = 0.1 mol dm^{-3} KCl) as samples, and a 5×10^{-5} mol dm^{-3} (μ = 0.1 mol dm^{-3} KCl) solution of the ligand as a reference.

HCl and KOH were used to adjust the pH values in all cases, which were measured on a Crison 2002 micro-pH meter.

4.7. NMR spectroscopy

^{1}H (300.13 MHz) and ^{13}C (75.48 MHz) spectra of H_3L and H_3L/Cd^{2+} mixtures in 1:1 molar ratios ([H_3L = 0.07 mmol dm^{-3}]) in D_2O solution, at several pH values were recorded at 298 K on a Bruker DPX300 spectrometer. ^{1}H–^{1}H and ^{13}C 2D correlation experiments were performed to assign the signals. Small amounts of 0.001 mol dm^{-3} NaOD or DCl solutions were added to a solution of H_3L to adjust the pD. The pH was calculated from the measured pD values using the following relationship pH = pD − 0.40 [29].

Acknowledgement

Financial support from the Spanish Ministerio de Ciencia y Tecnología (CTQ 2004-03332) is gratefully acknowledged.

Appendix A. Supplementary material

CCDC 652099 contains the supplementary crystallographic data for $\{[Cd(HL)H_2O]\cdot 3H_2O\}_n$. These data can be obtained free of charge via http://www.ccdc.cam.ac.uk/conts/retrieving.html, or from the Cambridge Crystallographic Data Centre, 12 Union Road, Cambridge CB2 1EZ, UK; fax: (+44) 1223-336-033; or e-mail: deposit@ccdc.cam.ac.uk.

References

[1] P.M. Cheremisinoff, C. Ellerbusch, Carbon Adsorption Handbook, Ann Arbor Science, Michigan, 1978.

[2] P.A. Brown, S.A. Gill, S.J. Allen, Water Res. 31 (2000) 3907.
[3] K. Csobàn, M. Pàrkànvi-Berka, P. Joo, P. Behra, Colloid Surf. A: Physicochem. Eng. Aspects 111 (1998) 347.
[4] J. García-Martín, R. López-Garzón, M. Luz Godino-Salido, M. Dolores Gutiérrez-Valero, P. Arranz-Mascarós, R. Cuesta, F. Carrasco-Marín, Langmuir 21 (2005) 6908.
[5] Javier García-Martín, Rafael López-Garzón, Maria Luz Godino-Salido, Rafael Cuesta-Martos, Maria Dolores Gutiérrez-Valero, Paloma Arranz-Mascarós, Helen Stoeckli-Evans, Eur. J. Inorg. Chem. (2005) 3093.
[6] M.D. Gutiérrez Valero, M. Luz Godino Salido, Paloma Arranz Mascarós, Rafael López Garzón, Rafael Cuesta, Javier García Martín, Langmuir 23 (2007) 5995.
[7] G.M. Sheldrick, Acta Crystallogr. A46 (1990) 467.
[8] Paloma Arranz Mascarós, M. Dolores Gutiérrez Valero, John N. Low, Christopher Glidewell, Acta Crystallogr. Sect. C 59 (2003) o210.
[9] M. Melguizo, A. Marchal, M. Nogueras, A. Sánchez, J.N. Low, J. Heterocyclic Chem. 39 (2002) 97.
[10] J.N. Low, M.D. López, P. Arranz-Mascarós, R. López-Garzón, M.D. Gutiérrez-Valero, M. Melguizo, G. Ferguson, C. Glidewell, Acta Crystallogr. B56 (2000) 882.
[11] Jussara Lopes de Miranda, Judith Felcman, Polyhedron 22 (2003) 225.
[12] A. Bencini, A. Bianchi, E. García-España, M. Micheloni, J.A. Ramirez, Coord. Chem. Rev. 88 (1999) 97.
[13] R. López Garzón, P. Arranz Mascarós, M.L. Godino Salido, M.D. Gutiérrez Valero, R. Cuesta, J.M. Moreno, Inorg. Chim. Acta 355 (2003) 41.
[14] R. López Garzón, M.L. Godino Salido, P. Arranz Mascarós, M.A. Fontecha Cámara, M.D. Gutiérrez Valero, R. Cuesta, J.M. Moreno, H. Stoekli Evans, Inorg. Chim. Acta 357 (2004) 2007.
[15] M.D. Gutiérrez Valero, R. López Garzón, P. Arranz Mascarós, M.D. López León, M.L. Godino Salido, Carbon (submitted for publication).
[16] P. Gans, A. Sabatini, A. Vacca, Talanta 43 (1996) 1739.
[17] A.E. Martell, R.M. Smith, R.J. Motekaitis, NIST Critically Selected Stability Constants of Metal Complexes Database, Version 7, Texas A&M University, College Station, TX, 2003.
[18] J.M. Moreno, P. Arranz Mascarós, R. López, M.D. Gutiérrez Valero, M.L. Godino Salido, J. Cobo Domingo, Polyhedron 18 (1999) 1635.
[19] C. Kallay, K. Varnagy, G. Micera, D. Scanna, I. Sovago, J. Inorg. Biochem. 99 (2005) 1514.
[20] P. Arranz Mascarós, M.L. Godino Salido, R. López Garzón, M.D. Gutiérrez Valero, J.M. Moreno Sánchez, Polyhedron 18 (1999) 689.
[21] W.J. Puspita, A. Odani, O. Yamauchi, J. Inorg. Biochem. 73 (1999) 203.
[22] R. López Garzón, P. Arranz Mascarós, M.L. Godino Salido, M.D. Gutiérrez Valero, J. Cobo Domingo, J.M. Moreno, Inorg. Chim. Acta 308 (2000) 59.
[23] J.N. Low, Paloma Arranz, Justo Cobo, M. Ángeles Fontecha, M. Luz Godino, Rafael López Garzón, Christopher Glidewell, Acta Crystallogr. C57 (2001) 534.
[24] J.N. Low, Paloma Arranz, Justo Cobo, M. Angeles Fontecha, M. Luz Godino, Rafael López Garzón, Debbie Cannon, Antonio Quesada, Christopher Glidewell, Acta Crystallogr. C57 (2001) 680.
[25] J.M. Salas-Peregrín, M.N. Moreno-Carretero, E. Colacio-Rodriguez, Can. J. Chem./Rev. Can. Chim. 63 (12) (1985) 3573.
[26] Stoe., IPDS Software, Stoe & Cie GmbH, Darmstadt, Germany, 2000.
[27] A.L. Spek, J. Appl. Crystallogr. 36 (2003) 7.
[28] M.L. Godino-Salido, M.D. Gutiérrez-Valero, R. López-Garzón, J.M. Moreno-Sánchez, Inorg. Chim. Acta 221 (1994) 177.
[29] A.K. Covington, M. Paabo, R.A. Robinson, R.G. Bates, Anal. Chem. 40 (1968) 700.